

Phase-Pure Epitaxial b-Axis-Oriented Bronze TiO₂ Films

Andreas Herklotz ¹, Frank Herklotz ² and Florina Stefania Rus ^{3,*}¹ Institute of Physics, Martin-Luther-University Halle-Wittenberg, 06120 Halle, Germany² Institute of Applied Physics, Technische Universität Dresden, 01069 Dresden, Germany³ National Institute for Research and Development in Electrochemistry and Condensed Matter, 300569 Timisoara, Romania

* Correspondence: rusflorinastefania@gmail.com

Abstract: We demonstrate the heteroepitaxial growth of phase-pure bronze-phase TiO₂ films using pulsed laser deposition on MgAl₂O₄ single-crystal substrates. While the growth on cubic substrates with smaller lattice parameters favors the stabilization of an out-of-plane-oriented anatase phase, and the use of substrates with larger lattice parameters leads to formation of the rutile phase, MgAl₂O₄ lies in a narrow intermediate range where the bronze phase is stabilized. X-ray diffraction shows that the b-axis is oriented out-of-plane, while the a–c lattice plane lies within the film plane. The bronze films show twinned domains due to their monoclinic structure that are aligned along all four in-plane directions of the MgAl₂O₄ lattice. In a subsequent step, TiO₂ films are grown on top of MgAl₂O₄-buffered MgO single crystals in order to demonstrate a route to stabilize the bronze phase on a larger variety of substrates. The growth of bronze-type TiO₂ films with the unique, open, one-dimensional framework aligned along the film normally may allow for the investigation of its basic functional properties related to ion diffusion that cannot otherwise be studied easily in other crystal forms.

Keywords: titanium dioxide; TiO₂(B); pulsed laser deposition; single crystal; MgAl₂O₄; spinel



Citation: Herklotz, A.; Herklotz, F.; Rus, F.S. Phase-Pure Epitaxial b-Axis-Oriented Bronze TiO₂ Films. *Appl. Sci.* **2023**, *13*, 209. <https://doi.org/10.3390/app13010209>

Academic Editor: Maria Amélia Ramos Loja

Received: 2 December 2022

Revised: 20 December 2022

Accepted: 21 December 2022

Published: 24 December 2022



Copyright: © 2022 by the authors. Licensee MDPI, Basel, Switzerland. This article is an open access article distributed under the terms and conditions of the Creative Commons Attribution (CC BY) license (<https://creativecommons.org/licenses/by/4.0/>).

1. Introduction

Among all transition metal oxides, titanium dioxide is one of the best studied and most used materials in industry [1]. A number of polymorphs of TiO₂ are known that differ in their physical properties and make them appealing for various applications. The three main polymorphs that are frequently encountered in nature are the rutile, anatase and brookite phases. All of these three phases are still heavily investigated in photocatalytic [2,3] and solar-cell applications [4,5], and improvement of their performances typically requires an optimized phase mixture. A fourth naturally occurring, far less well studied, polymorph is bronze-type TiO₂. This modification is the least dense of the four natural polymorphs of TiO₂, so it seems to be an excellent host for Li intercalation [6]. The bronze-type structure has one-dimensional open channels along the [010] direction that offer a good path for ion transport [7]. Bronze-TiO₂ has therefore, for example, been considered as a candidate anode material for lithium-ion batteries [8–10]. Because of its metastable properties, only a few investigations have been carried out in the electrochemistry field. These publications have indicated great potential in applications when several intrinsic drawbacks, such as moderate electrochemical kinetics and unsatisfactory long-cyclic stability, can be resolved [11].

The preparation of phase-pure crystals with well-defined surfaces is a prerequisite to understanding the potential of bronze-type TiO₂ for future applications. However, the preparation of phase-pure epitaxial films has been a challenge. Coexistence with one of the three more thermodynamically stable polymorphs is commonly observed [12]. Advances have recently been made in thin film heterostructures where the insertion of suitable buffer layers has allowed for the stabilization of epitaxial single-phase bronze films [13–15]. These films are c-axis oriented, which puts the one-dimensional ion channels in the film plane.

Here, we show that phase-pure bronze-type TiO_2 films can be prepared using pulsed laser deposition on single-crystal MgAl_2O_4 substrates without the need of a buffer layer. Our films are b-axis out-of-plane oriented and might thus serve as an ideal system to study fundamental properties of bronze-like TiO_2 related to ion migration.

2. Experimental Procedure

TiO_2 thin films with a thickness of 300 nm were grown on single-crystalline (001)-oriented LaAlO_3 (LAO), MgO and MgAl_2O_4 (MAO) substrates using pulsed laser deposition. A KrF excimer laser with a wavelength of 248 nm was used at an energy density of 2.0 J/cm^2 and a repetition rate of 2 Hz. The target was a stoichiometric ceramic rutile TiO_2 pellet. The growth temperature was $700 \text{ }^\circ\text{C}$. The growth was carried out in an oxygen pressure of 100 mbar, and the films were subsequently annealed for 20 min at the deposition temperature and cooled in 0.5 atm O_2 to ensure a good oxygen stoichiometry. Additionally, a TiO_2 film was grown on MgAl_2O_4 -buffered MgO substrates. The 50 nm thick buffer layers were deposited from a MAO substrate under the same conditions as mentioned above. Structural characterization of the films was carried out via X-ray diffraction (XRD) using a Bruker D8 Discover diffractometer. The optical properties of the TiO_2 films were determined using variable angle spectroscopic ellipsometry (VASE). The ellipsometric data were collected with a J.A. Woollam Co. ellipsometer working in rotating analyzer mode in the energy range of $1.2 \text{ eV} < h\nu < 5.0 \text{ eV}$ at incidence angles of 65° , 70° and 75° and at room temperature.

3. Results and Discussion

3.1. Phase Identification and Epitaxy

Figure 1 shows wide-angle XRD 2θ - θ scans of a set of TiO_2 films grown on the three substrates. The film on LAO is phase-pure and exhibits a very intense film peak at 38° . This film's peak can be assigned to the 004 peak of highly crystalline, out-of-plane-oriented anatase, which has been shown to stabilize on LAO substrates in prior work due to the favorable lattice mismatch [16,17]. On the contrary, the film on MgO is of poor structural quality and shows only a weak peak that can be assigned to the rutile 110 reflection. Thus, this film appears to be epitaxial, with the crystallographic c-axis within the film plane. Previous publications on TiO_2/MgO films have revealed rutile phases, or rutile/anatase mixtures as well, with the crystallinity strongly dependent on growth conditions [18,19]. The XRD scan of TiO_2/MAO shows only one film peak at $\sim 48.5^\circ$ over the entire scan range from 10 to 90° . We conclude that this film is single-crystalline. It is shown below that the film on MAO is phase-pure and of bronze type.

TiO_2 is known for having a plethora of polymorphs in close energetical proximity. Here, we focus on the four main polymorphs that are frequently observed experimentally, i.e., rutile, anatase, brookite and bronze. In order to rule out the stabilization of a more unique TiO_2 phase, we also considered all experimentally observed TiO_2 phases listed in the Crystallography Open Database [20] as well as all theoretically predicted structures listed in the Open Quantum Materials Database [21]. However, none of these phases are in agreement with our XRD data.

Figure 2 shows pole figures at the 2θ values of prominent reflections for each of the four main polymorphs. It can be seen that no film peaks are observed for the 110 rutile and 111 brookite reflections. These phases are not present in crystalline form. The situation is more complex for the anatase and bronze phases. In both pole figures, film peaks are visible, and it is not immediately clear if the film is phase-pure or if an anatase/bronze mixture is present. Virtually all lattice reflections of the anatase phase are at 2θ values that are in the vicinity of lattice reflections of the bronze phase. This fact makes it difficult to discern the two phases solely by the presence of certain film peaks. For example, the peak at $2\theta \sim 48.5^\circ$ can be associated with the 020 reflection of the bronze phase that, in bulk bronze- TiO_2 , would be located at $2\theta \sim 48.7^\circ$. However, the 200 reflection of bulk anatase is located at $2\theta \sim 48.3^\circ$. These small differences in the experimentally observed value could

be easily attributed to stress induced by the lattice, a thermal expansion mismatch to the substrate or slight non-stoichiometry.

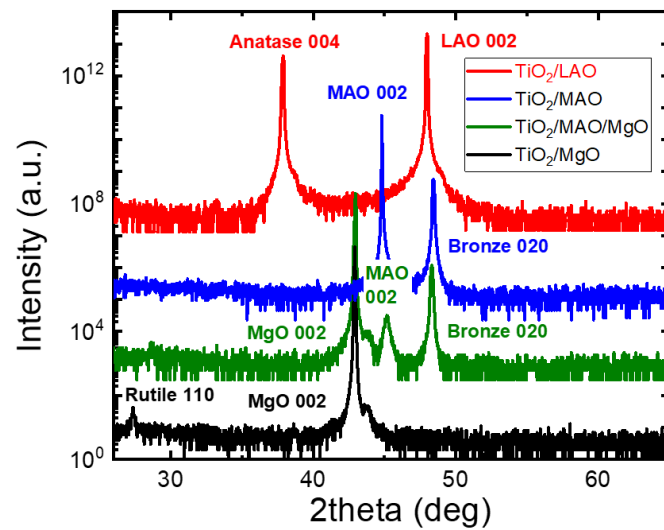


Figure 1. 2θ - θ scans of TiO_2 films grown on various substrates. While high-quality epitaxial anatase and low-quality polycrystalline rutile are crystallized on LAO and MgO substrates, respectively, it will be shown that phase-pure bronze TiO_2 is stabilized on MAO substrates and buffer layers.

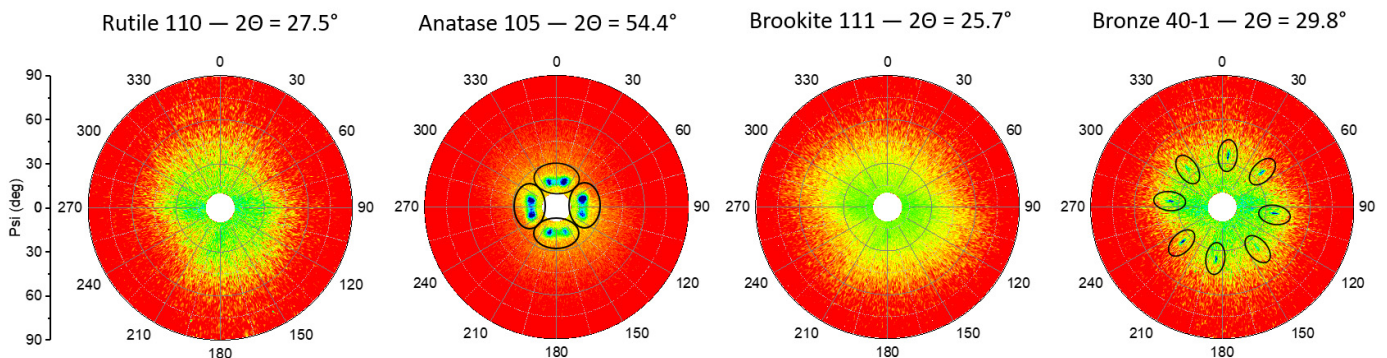


Figure 2. Pole figures around prominent reflections of each of the four main TiO_2 polymorphs considered. The reflections and their corresponding 2θ values are given. Film peaks are highlighted by black circles.

In order to separate the anatase and bronze phases, their epitaxial relationship to the substrate needs to be considered. Figure 3a shows a scan of the rotational goniometer axis φ at $2\theta = 25.1^\circ$ and the goniometer tilting angle $\phi = 18^\circ$. A double peak profile with four-fold symmetry can be seen. The peaks are rotated by $\pm 18^\circ$ with respect to the cubic substrate axis. There are two possible scenarios that are in agreement with the XRD data shown in Figures 1, 2 and 3a. They are illustrated in Figure 3b,c. In case one, the film is a b-axis, out-of-plane-oriented bronze film, with the a-axis aligned along the [100] and [010] in-plane axis of the cubic MAO substrates (Figure 3b). This arrangement provides a favorable lattice match along the a-lattice direction, since the lattice parameter of the bronze unit cell $a = 12.16 \text{ \AA}$ is only slightly larger (0.2%) than $3/2$ of the cubic lattice parameter of $\text{MAO}_{\text{aMAO}} = 8.09 \text{ \AA}$. The parallel and perpendicular components of the c-lattice vector with respect to the a-lattice vector are 2.00 \AA and 6.20 \AA , respectively, and, thus, about $1/4$ and $3/4$ of the MAO lattice parameter. In case two, the TiO_2 film is an in-plane-oriented anatase film. Here, the lattice mismatch would be minimized by aligning the c-axis along the [130] MAO lattice direction (Figure 3c).

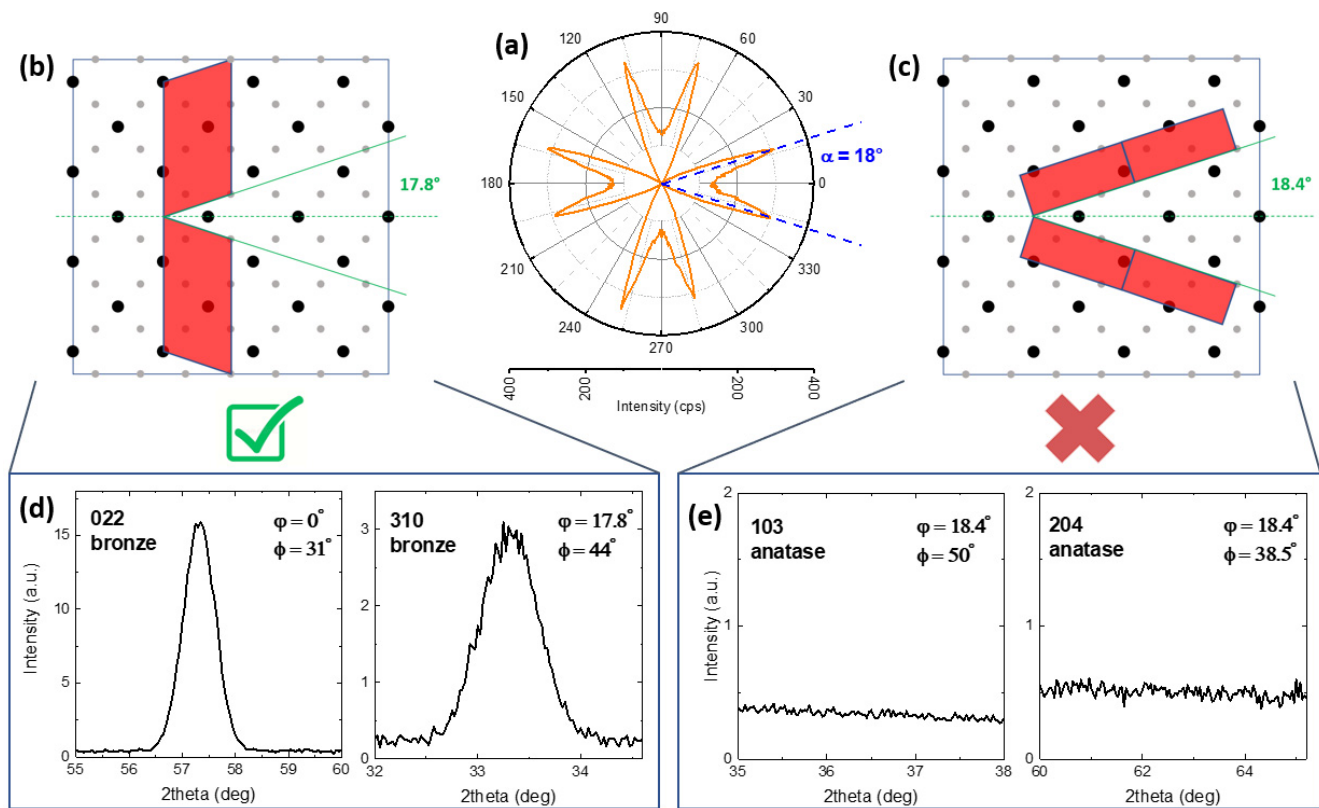


Figure 3. (a) φ -scan at $2\theta = 25.1^\circ$ and $\varphi = 18^\circ$. At these goniometer parameters, the 110 reflection of a b-axis-oriented bronze film and the 101 reflection of an a-axis-oriented anatase film would be expected. The two epitaxial configurations are illustrated in (b,c), respectively. In both cases, twinning would lead to a double peak structure with 4-fold symmetry as seen in (a). The stabilization of the bronze phase is confirmed via 2θ scans around the 022 and 310 bronze reflections, as shown in (d). (e) Scans along the 103 and 204 anatase reflections show no film peaks and indicate that no anatase is present.

In case one, the $\{110\}$ film peak family with four-fold symmetry is expected to be at $\varphi +/ - 17.8^\circ$, i.e., the monoclinic unit cell angle of the bronze structure. In case two, the angle would be expected to be $\arctan(1/3) = 18.4^\circ$. Figure 3d shows 2θ - θ scans around the bronze 310 and 022 reflections. Both film peaks are clearly present. This fact confirms the presence of b-oriented bronze. On the other hand, as can be seen in Figure 3e, no film peaks are observed around the anatase 103 and 204 reflections. We conclude that case two can be ruled out and that no anatase is present in the TiO_2 film. The film is of pure bronze phase.

3.2. Stability Range from First-Principle Calculations

MAO appears to be an ideal substrate choice for the stabilization of bronze TiO_2 . Its lattice only leads to a small mismatch of -0.2% along the a-axis and $+1.6\%$ and -2.2% along the parallel and perpendicular components of the c-axis, respectively. An only slightly smaller or larger lattice parameter would result in a larger mismatch in one of the two lattice directions and would increase stress substantially. In order to demonstrate that the crystal lattice of MAO favors the stabilization of the b-oriented bronze phase, we have performed first-principle density functional theory (DFT) calculations. All calculations have been conducted with the Quantum Espresso software package [22,23] and are based on Perdew–Burke–Ernzerhof (PBE) exchange functionals and a $4 \times 4 \times 4$ Monkhorst k-point grid. Projector-augmented wave pseudopotentials with an energy cut-off of 680 eV were employed.

In order to study the effect of epitaxy, the unit cells of the three observed TiO₂ polymorphs are fixed to a square lattice with varying lattice parameters, as they would be forced by epitaxially strained growth on cubic single-crystal substrates. Unit cell planes are constrained to match the substrates' square lattice, while the out-of-plane lattice parameters and all internal coordinates are free to relax. For all phases, the epitaxial relationships revealed through XRD were addressed. Additionally, for rutile we have considered the case of biaxial strain within the a–b plane. All other epitaxial relationships have been ruled out due to their large lattice mismatches.

The result of the calculations is shown in Figure 4. The bronze phase is most stable in a narrow lattice parameter range around that of the MAO substrate. For smaller lattice parameters, as, for example, for LAO and SrTiO₃, the anatase phase is more stable. This is in agreement with our experimental observation. According to our calculations, a rutile phase with the (110) face epitaxially strained to the substrate is the most stable for larger lattice parameter $a_{\text{sub}} > 4.19 \text{ \AA}$. This fact matches with our experimental observation of (110)-oriented rutile films on MgO as well. It should be mentioned that this epitaxial configuration favors twinning, and the lattice mismatch of rutile to MgO is still substantial. Film growth with minor structural quality can be expected. In conclusion, our DFT calculations are in good agreement with our experiments and provide justification for why the stabilization of the bronze phase has not been observed as single layer on any other substrate yet.

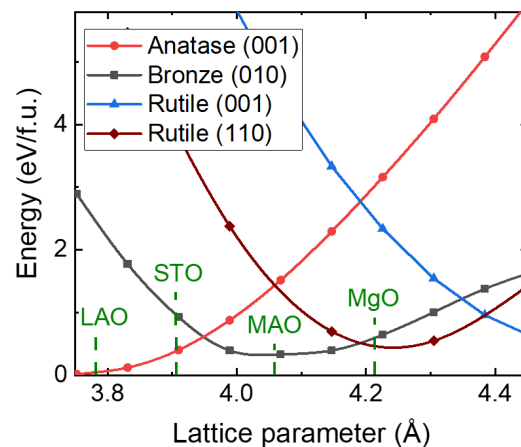


Figure 4. Calculated total energies per formula unit of TiO₂ as a function of the in-plane lattice parameter a_{sub} . The epitaxial relationships considered are biaxial strains within in the anatase (001) plane, bronze (010) plane, rutile (001) plane and rutile (110) plane. Pseudocubic lattice parameters of standard single-crystal substrates are marked for reference. The total energies are given with respect to the ground state energy of the anatase bulk structure.

3.3. MAO as Thin Film Template

MAO is a cheap, transparent, non-magnetic, chemically stable and easily available substrate material. Despite these advantages, there might be other reasons to use substrates that do not allow for the growth of phase-pure bronze films directly. Using MAO buffer layers can circumvent this issue and possibly enable the growth of bronze films on a large variety of standard crystals. In Figure 1, this fact is demonstrated by the growth of a TiO₂(B)/MAO/MgO heterostructure. The bronze film is b-axis-oriented and phase-pure.

3.4. Optical Properties

Variable-angle spectroscopic ellipsometry was used to demonstrate the different optical properties of the TiO₂ films. The energy-dependent ellipsometric angles Ψ and Δ were recorded for all three single-layer samples. The data were then fit to a simple two-layer model consisting of the substrate and film in order to determine the optical properties of

the film. The substrate and the TiO₂ layer are approximated by a B-spline with 38 data points over the full energy range. Here, the optical properties of the substrates are first determined independently by fitting the VASE data of a bare substrate. Next, the recorded film-substrate VASE data were simulated by fitting the TiO₂ optical properties and leaving the substrate properties fixed.

Figure 5 shows a Tauc plot of the absorption coefficients α of the three single-layer films. Here, the square of α multiplied by the photon energy is drawn as a function of the photon energy. This Tauc-plot representation is typically used to determine direct optical band gaps by extrapolating the linear part to zero. For indirect band-gap materials, the square root instead of the square of the absorption coefficient would be used. It should be mentioned that our DFT calculations (not shown) as well as previous work indicate that bronze TiO₂ has a direct band gap. The same is true for rutile. Anatase is considered to be an indirect band-gap material. This fact indicates that the Tauc plot in Figure 5 is technically not suited to determine the exact band gap of the anatase film. However, we decided to present all the data in one single Tauc plot for comparability. It should be stressed that our main goal is not to determine exact band-gap values, but to highlight the strong differences in the optical properties between the thin film samples.

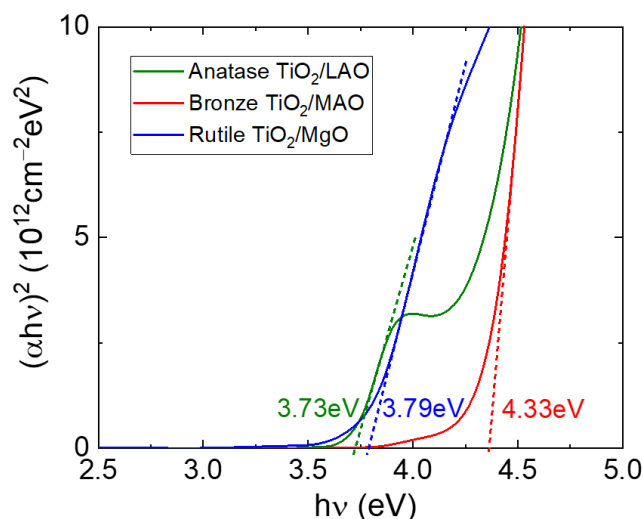


Figure 5. Tauc plot of the absorption coefficient α as function of the photon energy $h\nu$ for the single-layer TiO₂ films. The band gaps were determined by extrapolating the linear parts of the curves to zero. A clear difference between the bronze film and the other polymorphs can be seen.

Our experimental data show that, for the bronze film, the band gap (~4.3 eV) is at notably larger energies than that for anatase (3.7 eV) and rutile (3.8 eV). Little is known about the optical band gap of bronze TiO₂. First-principle calculations have placed the electronic band gap of the bronze phase at about 4.1 eV, and more than 0.5 eV above that of anatase and rutile [24]. Our data are therefore in good agreement with the theory. In the literature, the experimentally determined optical band gaps of bulk TiO₂ polymorphs vary quite a bit, with the values for anatase and rutile typically ranging between 3.1–3.4 eV and 3.0–3.3 eV, respectively [25]. Our experimental values on thin films are about 0.5 eV higher, mainly due to the method that was used to determine the band gaps [26]. Additionally, band gaps of thin films determined using ellipsometry have consistently been shown to be 0.1–0.2 eV higher than those determined using transmission spectroscopy [27], the standard technique used for bulk materials. Our data are, however, consistent with the work of Lee et al., the only experimental study known to us that reports on the optical properties of bronze-type epitaxial films [14]. In this report the optical band gap of bronze-type TiO₂ was also found to be about 0.5 eV higher than that of anatase. Figure 5 clearly demonstrates that the film on MAO has vastly different optical properties than the other two films and

corroborates the XRD analysis. Our results indicate that the epitaxial stabilization of bronze-type TiO₂ on MAO substrates would also allow for the investigation of other fundamental properties that otherwise cannot be studied due to the lack of phase-pure crystals.

4. Conclusions

Pulsed laser deposition has been used to grow thin films of TiO₂ on pseudocubic single-crystal substrates. We observe that different TiO₂ polymorphs can be stabilized dependent on the substrate choice. In particular, we find that phase-pure TiO₂ with a bronze structure can be stabilized on 001-oriented MgAl₂O₄ substrates. This fact is mostly deduced from four-circle XRD. Measurements of the absorption coefficient using ellipsometry confirm that the film grown on MAO is of a different phase than anatase or rutile and corroborate our observation of bronze TiO₂. The epitaxial stabilization of bronze films on other standard substrates has been notoriously difficult and has previously only been achieved by the insertion of additional buffer layers that improve the lattice match to the bronze structure but also add another layer of complexity to the growth of heterostructures. Additionally, in contrast to previous work, our films are b-axis, out-of-plane-oriented. This epitaxial relationship is ideal to study phenomena based on ion migration through the one-dimensional open channels along the [010] crystal direction.

Author Contributions: Conceptualization, A.H. and F.S.R.; methodology, A.H. and F.S.R.; software, A.H.; validation, A.H., F.H. and F.S.R.; formal analysis, A.H.; investigation, A.H.; resources, A.H. and F.S.R.; data curation, A.H. and F.S.R.; writing—original draft preparation, A.H.; writing—review and editing, A.H., F.H. and F.S.R.; visualization, A.H.; supervision, F.S.R.; project administration, A.H. and F.H.; funding acquisition, A.H. and F.H. and F.S.R. All authors have read and agreed to the published version of the manuscript.

Funding: A.H. was funded by the German Research Foundation (DFG)—Grant No. HE8737/1-1. F.H. was funded by the German Research Foundation (DFG)—Grant No. LA1397/20. The work of F.S.R. was supported by a mobility grant of the Romanian Ministry of Research and Innovation, CNCS—UEFISCDI, project number P1-1.1-MC-2018-0561, within PNCDI III.

Institutional Review Board Statement: Not applicable.

Informed Consent Statement: Not applicable.

Data Availability Statement: The study did not report any data.

Conflicts of Interest: The authors declare no conflict of interest.

References

- Haider, A.J.; Jameel, Z.N.; Al-Hussaini, I.H.M. Review on: Titanium Dioxide Applications. *Energy Procedia* **2019**, *157*, 17–29. [[CrossRef](#)]
- Dharma, H.N.; Jaafar, J.; Widiastuti, N.; Matsuyama, H.; Rajabsadeh, S.; Othman, M.H.; Rahman, M.A.; Jafri, N.N.; Suhaimin, N.S.; Nasir, A.M.; et al. A Review of Titanium Dioxide (TiO₂)-Based Photocatalyst for Oilfield-Produced Water Treatment. *Membranes* **2022**, *12*, 345. [[CrossRef](#)] [[PubMed](#)]
- Moma, J.; Baloyi, J. Modified Titanium Dioxide for Photocatalytic Applications. In *Photocatalysts*; Khan, S.B., Akhtar, K., Eds.; IntechOpen: Rijeka, Croatia, 2018; Chapter 3; ISBN 978-1-78985-476-3.
- Wis, G.; Sawicka-Chudy, P.; Wal, A.; Potera, P.; Bester, M.; Ploch, D.; Sibiński, M.; Cholewa, M.; Ruszala, M. TiO₂:ZnO/CuO thin film solar cells prepared via reactive direct-current (DC) magnetron sputtering. *Appl. Mater. Today* **2022**, *29*, 101673. [[CrossRef](#)]
- Sawicka-Chudy, P.; Wis, G.; Głowa, Ł.; Sibiński, M.; Potera, P.; Cholewa, M.; Wielgosz, M.; Górny, S. Optical and structural properties of TiO₂ as intermediate buffer layer prepared by DC reactive magnetron sputtering for solar cells. *Optik* **2019**, *181*, 1122–1129. [[CrossRef](#)]
- Rahimi, N.; Pax, R.A.; Gray, E. MacA. Review of functional titanium oxides. I: TiO₂ and its modifications. *Prog. Solid State Chem.* **2016**, *44*, 86–105. [[CrossRef](#)]
- Marchand, R.; Brohan, L.; Tournoux, M. TiO₂(B) a new form of titanium dioxide and the potassium octatitanate K₂Ti₈O. *Mater. Res. Bull.* **1980**, *15*, 1129–1133. [[CrossRef](#)]
- Armstrong, A.R.; Armstrong, G.; Canales, J.; Bruce, P.G. TiO₂-B nanowires as negative electrodes for rechargeable lithium batteries. *J. Power Sources* **2005**, *146*, 501–506. [[CrossRef](#)]
- Ren, Y.; Liu, Z.; Pourpoint, F.; Armstrong, A.R.; Grey, C.P.; Bruce, P.G. Nanoparticulate TiO₂(B): An Anode for Lithium-Ion Batteries. *Angew. Chem. Int. Ed.* **2012**, *51*, 2164–2167. [[CrossRef](#)]

10. Brutti, S.; Gentili, V.; Menard, H.; Scrosati, B.; Bruce, P.G. TiO₂-(B) Nanotubes as Anodes for Lithium Batteries: Origin and Mitigation of Irreversible Capacity. *Adv. Energy Mater.* **2012**, *2*, 322–327. [[CrossRef](#)]
11. Liang, S.; Wang, X.; Qi, R.; Cheng, Y.-J.; Xia, Y.; Müller-Buschbaum, P.; Hu, X. Bronze-Phase TiO₂ as Anode Materials in Lithium and Sodium-Ion Batteries. *Adv. Funct. Mater.* **2022**, *32*, 2201675. [[CrossRef](#)]
12. Zhang, K.; Du, X.; Katz, M.B.; Li, B.; Kim, S.J.; Song, K.; Graham, G.W.; Pan, X. Creating high quality Ca:TiO₂-B (CaTi₅O₁₁) and TiO₂-B epitaxial thin films by pulsed laser deposition. *Chem. Commun.* **2015**, *51*, 8584–8587. [[CrossRef](#)] [[PubMed](#)]
13. Guo, W.; Ji, D.X.; Yuan, Z.S.; Wang, P.; Nie, Y.F.; Gu, Z.B.; Pan, X.Q. Epitaxial growth of bronze phase titanium dioxide by molecular beam epitaxy. *AIP Adv.* **2019**, *9*, 035230. [[CrossRef](#)]
14. Lee, S.; Gao, X.; Sohn, C.; Ha, Y.; Yoon, S.; Ok, J.M.; Chisholm, M.F.; Noh, T.W.; Lee, H.N. Templated epitaxy of TiO₂(B) on a perovskite. *Appl. Phys. Lett.* **2020**, *117*, 133903. [[CrossRef](#)]
15. Jokisaari, J.R.; Bayerl, D.; Zhang, K.; Xie, L.; Nie, Y.; Schlom, D.G.; Kioupakis, E.; Graham, G.W.; Pan, X. Polarization-Dependent Raman Spectroscopy of Epitaxial TiO₂(B) Thin Films. *Chem. Mater.* **2015**, *27*, 7896–7902. [[CrossRef](#)]
16. Murakami, M.; Matsumoto, Y.; Nakajima, K.; Makino, T.; Segawa, Y.; Chikyow, T.; Ahmet, P.; Kawasaki, M.; Koinuma, H. Anatase TiO₂ thin films grown on lattice-matched LaAlO₃ substrate by laser molecular-beam epitaxy. *Appl. Phys. Lett.* **2001**, *78*, 2664–2666. [[CrossRef](#)]
17. Sakama, H.; Osada, G.; Tsukamoto, M.; Tanokura, A.; Ichikawa, N. Epitaxial growth of anatase TiO₂ thin films on LaAlO₃(100) prepared using pulsed laser deposition. *Thin Solid Films* **2006**, *515*, 535–539. [[CrossRef](#)]
18. Okimura, K.; Furumi, T. Epitaxial Growth of Rutile TiO₂ Films on MgO Substrate in Inductively Coupled Plasma-Assisted Sputtering. *Jpn. J. Appl. Phys.* **2004**, *43*, L655. [[CrossRef](#)]
19. Garapon, C.; Champeaux, C.; Mugnier, J.; Panczer, G.; Marchet, P.; Catherinot, A.; Jacquier, B. Preparation of TiO₂ thin films by pulsed laser deposition for waveguiding applications. *Appl. Surf. Sci.* **1996**, *96–98*, 836–841. [[CrossRef](#)]
20. Grazulis, S.; Chateigner, D.; Downs, R.T.; Yokochi, A.F.T.; Quiros, M.; Lutterotti, L.; Manakova, E.; Butkus, J.; Moeck, P.; Le Bail, A. Crystallography Open Database—an open-access collection of crystal structures. *J. Appl. Crystallogr.* **2009**, *42*, 726–729. [[CrossRef](#)]
21. Kirklin, S.; Saal, J.E.; Meredig, B.; Thompson, A.; Doak, J.W.; Aykol, M.; Rühl, S.; Wolverton, C. The Open Quantum Materials Database (OQMD): Assessing the accuracy of DFT formation energies. *Npj Comput. Mater.* **2015**, *1*, 15010. [[CrossRef](#)]
22. Giannozzi, P.; Baroni, S.; Bonini, N.; Calandra, M.; Car, R.; Cavazzoni, C.; Ceresoli, D.; Chiarotti, G.L.; Cococcioni, M.; Dabo, I.; et al. QUANTUM ESPRESSO: A modular and open-source software project for quantum simulations of materials. *J. Phys. Condens. Matter* **2009**, *21*, 395502. [[CrossRef](#)] [[PubMed](#)]
23. Giannozzi, P.; Andreussi, O.; Brumme, T.; Bunau, O.; Buongiorno Nardelli, M.; Calandra, M.; Car, R.; Cavazzoni, C.; Ceresoli, D.; Cococcioni, M.; et al. Advanced capabilities for materials modelling with Quantum ESPRESSO. *J. Phys. Condens. Matter* **2017**, *29*, 465901. [[CrossRef](#)] [[PubMed](#)]
24. Buckeridge, J.; Butler, K.T.; Catlow, C.R.A.; Logsdail, A.J.; Scanlon, D.O.; Shevlin, S.A.; Woodley, S.M.; Sokol, A.A.; Walsh, A. Polymorph Engineering of TiO₂: Demonstrating How Absolute Reference Potentials Are Determined by Local Coordination. *Chem. Mater.* **2015**, *27*, 3844–3851. [[CrossRef](#)]
25. Zhu, T.; Gao, S.-P. The Stability, Electronic Structure, and Optical Property of TiO₂ Polymorphs. *J. Phys. Chem. C* **2014**, *118*, 11385–11396. [[CrossRef](#)]
26. Zanatta, A.R. Revisiting the optical bandgap of semiconductors and the proposal of a unified methodology to its determination. *Sci. Rep.* **2019**, *9*, 11225. [[CrossRef](#)]
27. Sando, D.; Carrétero, C.; Grisolia, M.N.; Barthélémy, A.; Nagarajan, V.; Bibes, M. Revisiting the Optical Band Gap in Epitaxial BiFeO₃ Thin Films. *Adv. Opt. Mater.* **2018**, *6*, 1700836. [[CrossRef](#)]

Disclaimer/Publisher’s Note: The statements, opinions and data contained in all publications are solely those of the individual author(s) and contributor(s) and not of MDPI and/or the editor(s). MDPI and/or the editor(s) disclaim responsibility for any injury to people or property resulting from any ideas, methods, instructions or products referred to in the content.